Colchicine alleviates severe acute pancreatitis in rats by inhibiting acinar cell ferroptosis *via* LCN2/MAPK/ERK signaling axis

Liu Yang,[1] Xiaoyi Zheng,[2] Yang Zhang,[3] Yue Li,[4] Lei Li,[1] Feng Liu[1]

[1]Digestive Endoscopy Center, Shanghai Tenth People's hospital, School of Medicine, Tongji University, Shanghai
[2]General Hospital of Ningxia Medical University, Ningxia Hui Autonomous Region, Yinchuan
[3]Department of Ophthalmology, Ruijin Hospital Affiliated Medical School, Shanghai Jiaotong University, Shanghai
[4]Edibeck Therapeutics Company Limited, Shenzhen, China

ABSTRACT

Colchicine (COL) is known to ameliorate severe acute pancreatitis (SAP), yet the precise molecular mechanisms remain elusive. This study integrates bioinformatics with in vivo experimentation to elucidate the mechanism by which COL attenuates SAP. An SAP rat model was established via sodium taurocholate injection. Key therapeutic targets were screened using transcriptomics and network pharmacology. Mechanistic validation utilized AAV-mediated lipocalin-2 (LCN2) overexpression, the ferroptosis inhibitor ferrostatin-1 (Fer-1), and the ERK inhibitor PD98059. COL treatment significantly ameliorated pancreatic pathological injury, inflammatory cell infiltration, and cytokine release. LCN2 was identified as a pivotal target markedly upregulated in SAP but downregulated by COL. Crucially, LCN2 overexpression reversed COL's therapeutic benefits and restored ferroptosis markers (COX2, Fe^{2+}, ROS) while suppressing anti-ferroptotic indices. Notably, this reversal was effectively abrogated by co-treatment with either Fer-1 or PD98059, confirming the involvement of the MAPK/ERK pathway. This study is the first to elucidate that COL inhibits ferroptosis in pancreatic acinar cells by downregulating LCN2 and subsequently suppressing the LCN2/MAPK/ERK signaling axis. These findings provide a novel molecular basis for COL and highlight a potential target for therapeutic intervention in SAP.

Key words: Severe acute pancreatitis; colchicine; lipocalin-2; ferroptosis; ERK1/2.

Correspondence: Feng Liu, Shanghai Tenth People's Hospital, 301 Yanchang Middle Road, Jing'an District, Shanghai 200072, China. E-mail: 1905041@tongji.edu.cn
Lei Li, Shanghai Tenth People's Hospital, 301 Yanchang Middle Road, Jing'an District, Shanghai 200072, China. E-mail: raulowen84@hotmail.com

Contributions: Liu Yang, study protocol design, data collection, data analysis, literature search, writing – original drafting. Xiaoyi Zheng, Yang Zhang, Yue Li, Lei Li, Feng Liu, research management, contribution to funding acquisition and study management. All authors read and approved the final manuscript and agreed to be accountable for all aspects of the work.

Conflict of interest: the authors declare that the research was conducted in the absence of any commercial or financial relationships that could be construed as a potential conflict of interest.

Ethical approval: this study was approved by the Experimental Medicine Research Center of Ruijin Hospital Affiliated to Shanghai Jiao Tong University School of Medicine (Approval No. ADM-019-T01).

Funding: this work was supported by the National Natural Science Foundation of China (No. 82172572) and Shanghai Science and Technology Commission Foundation (No. 21S31903800).

Availability of data and materials: data generated or analyzed during this study are available from the corresponding author on reasonable request.

Introduction

Severe acute pancreatitis (SAP) constitutes the most perilous spectrum of acute pancreatitis, distinguished by its rapid clinical onset and the persistence of organ failure exceeding 48 hours. The pathophysiology of this condition is intricate, primarily fueled by the extensive necrosis of pancreatic acinar cells, which subsequently triggers systemic inflammatory response syndrome (SIRS) and multiple organ dysfunction syndrome (MODS).[1,2] Epidemiological data indicate that the annual incidence of acute pancreatitis varies between 5 and 80 per 100,000 individuals globally, with severe progression occurring in approximately 20-30% of these cases.[3] Despite recent strides in deciphering the pathogenesis and clinical management of SAP, patient prognosis remains unsatisfactory. Consequently, there is a critical need to discover innovative therapeutic targets and intervention tactics.

Colchicine (COL), a natural alkaloid extracted from the seeds and bulbs of *Colchicum autumnale* (Liliaceae), is clinically established for the treatment of acute gout and familial Mediterranean fever.[4,5] Its canonical anti-inflammatory mechanism involves the inhibition of microtubule polymerization, which impairs neutrophil chemotaxis and migration, thereby attenuating leukocyte infiltration and the release of inflammatory mediators.[6] Beyond this, COL has been shown to suppress cytokine release *via* the NLRP3 inflammasome pathway and is widely utilized in treating inflammatory conditions such as Behçet's disease and recurrent stomatitis.[7,8] Recent evidence highlights its potential for drug repurposing; for instance, Zhang *et al.* reported that COL binds to the shank protein to inhibit macrophage polarization toward the pro-inflammatory M1 phenotype while promoting the anti-inflammatory M2 phenotype.[9]

Ferroptosis represents a distinct form of regulated cell death propelled by iron-dependent lipid peroxidation, marked by intracellular iron overload and the accretion of reactive oxygen species (ROS). Ultrastructurally, it manifests as mitochondrial atrophy with increased membrane density.[10] Within the landscape of acute pancreatitis, acinar cells show heightened vulnerability to iron metabolic dysregulation and compromised glutathione peroxidase 4 (GPX4) activity, resulting in a lethal buildup of lipid peroxides.[11] Liu and colleagues established a correlation between SAP and ferroptosis, noting that in SAP models, protective factors like glutathione (GSH) and superoxide dismutase (SOD) were depleted, whereas malondialdehyde (MDA) and hydrogen peroxide (H_2O_2) levels surged. This biochemical shift was accompanied by Acsl4 upregulation and the suppression of Gpx4 and Slc7a11.[12] Therefore, targeting the ferroptotic cascade offers a promising therapeutic avenue for SAP.

Lipocalin-2 (LCN2) is a secretory protein intricately linked to iron homeostasis and plays a pivotal role in inflammation, oxidative stress, and cell death.[13] Emerging evidence suggests that LCN2 functions as a critical regulator of ferroptosis across various pathologies. For example, in cerebral ischemia-reperfusion injury, LCN2 promotes endothelial ferroptosis *via* HMGB1/NRF2/HO-1 axis, exacerbating blood-brain barrier dysfunction.[14] Similarly, in age-related macular degeneration, LCN2 binds to ATG4B in the retinal pigment epithelium and forms a complex with LC3B, disrupting autophagosome maturation and lysosomal function, leading to iron accumulation and activation of the cGAS-STING pathway, thereby promoting oxidative stress and iron death.[15] These precedents suggest that LCN2 may serve as a crucial molecular nexus connecting inflammatory injury to ferroptosis.

Our previous investigations demonstrated that in a sodium taurocholate (STC)-induced SAP rat model, COL treatment significantly ameliorated pancreas and lung injury by suppressing inflammation, apoptosis, and oxidative stress. However, the precise molecular mechanisms underlying these protective effects remain to be fully elucidated. In the present study, we employed an integrative approach combining whole-transcriptome sequencing (RNA-Seq) of the pancreas from Sham, SAP, and COL-treated rats with network pharmacology and *in vivo* validation. We aim to screen for critical targets of COL and systematically elucidate the molecular mechanism by which COL inhibits ferroptosis and alleviates SAP via the regulation of the LCN2-mediated signaling axis.

Materials and Methods

Animals and experimental protocols

Healthy male Sprague-Dawley (SD) rats (280-320 g, aged 6-8 weeks) were sourced from Shanghai Vital River Laboratory Animal Technology Co., Ltd. (Shanghai, China) and housed in a specific pathogen-free (SPF) environment. The study design incorporated three separate experimental cohorts:

Cohort 1: rats were distributed into three groups (n=6): Sham, SAP, and SAP+COL. For the SAP+COL group, COL (0.5 mg/kg/d; Sigma-Aldrich, St. Louis, MO, USA) was administered *via* intragastric gavage for seven consecutive days. The Sham and SAP groups were given a matching volume of saline. On day 7, one h post-gavage, SAP was established by injecting 5% STC (1 mL/kg, 20 μL/min) into the biliopancreatic duct in a retrograde manner. The Sham group was subjected to the same surgical manipulation without induction.

Cohort 2: rats were divided into six groups (n=5): Sham, SAP, SAP+COL, SAP+COL+OE-CTR, SAP+COL+OE-LCN2, and SAP+COL+OE-LCN2+Fer-1. To facilitate pancreatic overexpression, pancreas-targeted adeno-associated virus (AAV/PAN-OE-LCN2 or AAV/PAN-OE-CTR; $2*10^{12}$ vg/rat; Obio Technology, Shanghai, China) was injected intraperitoneally into the OE groups two weeks ahead of the COL treatment. In the SAP+COL+OE-LCN2+Fer-1 group, Fer-1 (10 mg/kg; Selleck, Houston, TX, USA) treatment occurred *via* intraperitoneal injection 1 h prior to inducing SAP.

Cohort 3: this cohort followed the structure of Cohort 2 (n=5), with a modification in the final group: SAP+COL+OE-LCN2+PD98059. Here, the ERK1/2 inhibitor PD98059 (10 mg/kg; Selleck, USA) was applied intraperitoneally 1 h before the SAP procedure.

Tissue and serum samples were harvested after euthanizing the animals, 24 h post-biliary duct catheterization. All procedures adhered to protocols authorized by the Experimental Medicine Research Center of Ruijin Hospital, Affiliated to Shanghai Jiao Tong University School of Medicine (Ethics approval: ADM-019-T01).

Histology and immunofluorescence assessments

Pancreatic and pulmonary tissues were fixed in 4% paraformaldehyde, embedded in paraffin, and sectioned (4 μm). H&E staining was performed to evaluate pathological injury (edema, inflammation, necrosis), scored on a 0-3 scale.[16] For Immunohistochemistry (IHC) and immunofluorescence (IF), sections underwent antigen retrieval and blocking with 5% BSA. Primary antibodies against LCN2 (1:200; PB9609, Boster, Wuhan, China), MMP9 (1:200; AF5228, Affinity, Waltham, MA, USA), IL-6 (1:200; BA4339, Boster), MPO (1:200; ab208670, Abcam,

Cambridge, MA, USA), or CD68 (1:200; ab283654, Abcam) were incubated overnight at 4°C. Secondary antibodies (Alexa Fluor 488/594 for immunofluorescence) were applied for 1 h. Images were acquired using a fluorescence microscope.

qRT-PCR

TRIzol reagent (Invitrogen, Carlsbad, CA, USA) served to isolate total pancreatic RNA. cDNA synthesis was performed using the HiScript III RT SuperMix for qPCR (+gDNA wiper) (Vazyme, Nanjing, China). qRT-PCR was conducted on a LightCycler 480 II system (Roche, Basel, Switzerland) using ChamQ Universal SYBR qPCR Master Mix (Vazyme, Nanjing, China). Relative mRNA expression was normalized to *GAPDH*.

The primer sequences were as follows: *Lcn2*: Forward: 5'-CTTGTCCTGCTTGGGGTCCTG-3', Reverse: 5'-CACCTGCCCTGGAACCGTTC-3'*; Mmp9*: Forward: 5'-CAAACCCTGCGTATTTCCATTCATC-3', Reverse: 5'-GATAACCATCCGAGCGACCTTTAG-3'*; GAPDH*: Forward: 5'-GGCAAGTTCAACGGCACAGTC-3', Reverse: 5'-TCGCTCCTGGAAGATGGTGATG-3'.

Western blot analysis

Pancreas (20 mg) was homogenized in RIPA buffer with PMSF. Protein concentrations were determined *via* BCA Assay (P0010, Beyotime, Shanghai, China). Samples (25 μg) were resolved on 15% SDS-PAGE gels and transferred to PVDF membranes (Millipore, Billerica, MA, USA). Following blockage with 5% non-fat milk, membranes were incubated overnight at 4°C with primary antibodies against GAPDH (1:2000, Proteintech, Rosemont, IL, USA), GPX4 (1:1000, Abcam), FTH (1:1000, Abcam), COX2 (1:1000, Abcam), ERK1/2 (1:1000, Cell Signaling Technology, Danvers, MA, USA), p-ERK1/2 (1:1000, Cell Signaling Technology), and LCN2 (1:1000, Abclonal, Wuhan, China). Secondary HRP-conjugated antibodies (1:2000, Cell Signaling Technology,) were applied for 1 hour. Bands were visualized with an ECL kit (Beyotime) on the SCG-W3000 PLUS system (Servicebio, Wuhan, China), and ImageJ software facilitated densitometry.

Serum biochemistry and ELISA

Serum was separated by centrifugation (3000 g, 10 min). Amylase and lipase activities were measured using commercial kits (C016-1-1/A054-2-1, Nanjing Jiancheng, Nanjing, China). Serum levels of IL-1β, IL-6, and TNF-α were measured using ELISA kits (A1010A0301b/A1010A0306/A1010A0320S, BioTNT, Shanghai, China), and serum LCN2 was detected using a specific ELISA kit (E-EL-R3055, Elabscience, Wuhan, China) according to the manufacturers' instructions.

Bioinformatics and RNA-Seq

After extracting total RNA from the Sham, SAP, and SAP+COL groups, rRNA was depleted *via* the Ribo-off Kit (Vazyme, Nanjing, China). Oebiotech Co. (Shanghai, China) handled library construction (VAHTS Universal V6 Kit) and sequencing (Illumina Novaseq 6000). Trimmomatic was used to filter raw data. The limma R package was employed for differential expression profiling ($|\log_2$ Fold change$|$ >2, nominal, $p<0.05$). Visualization utilized ggplot2 (volcano plots) and pheatmap(heatmaps). We used Venn diagrams to pinpoint intersecting genes. clusterProfiler facilitated GO and KEGG enrichment analyses (FDR <0.25, $p<0.05$).

PPI network and hub gene identification

A PPI network was established using the STRING database (V12.0) to explore interactions within DEGs-1. Visualization was achieved *via* Cytoscape (V3.10.2). To distinguish hub genes, we applied the MCODE plug-in alongside five topological algorithms (Closeness, Degree, EPC, MNC, Radiality) provided by the CytoHubba plug-in.

Network pharmacology strategy

Potential therapeutic targets of COL were identified using the PharmMapper server (https://www.lilab-ecust.cn/pharmmapper/index.html). The 3D chemical structure file of Colchicine was uploaded for pharmacophore mapping, and targets exhibiting a normalized fit score >0.8 were retained as significant candidates. To construct a comprehensive inventory of disease-associated targets, the OMIM (https://www.omim.org/) and GeneCards (https://www.genecards.org/) databases were queried using the search terms «severe acute pancreatitis» and «acute pancreatitis». The retrieved datasets from these sources were merged, and duplicate entries were eliminated to establish a definitive SAP-related target set. Gene symbols and protein nomenclature were standardized using the UniProt database (https://www. uniprot.org/) to ensure consistency. Ultimately, this screening process yielded 290 putative targets for COL and 3,925 SAP-associated targets.

Assessment of ROS, GSH/GSSG, MDA, and Fe2+

An ROS Assay Kit (Beyotime, Shanghai, China) was used to gauge pancreatic ROS. Fresh tissue was flash-frozen in O.C.T., cryosectioned (8 μm), and fixed. Sections were incubated with the fluorescent probe (37°C, 30 min) following PBS washing. DAPI counterstaining was performed, and images were captured via fluorescence microscopy (Nikon, Tokyo, Japan).

For biochemical assays, protein concentration in pancreatic supernatants was determined by BCA for normalization. The GSH/GSSG ratio was derived from levels quantified by an enzymatic recycling kit (Beyotime). Lipid peroxidation was evaluated *via* MDA content (TBA method, Nanjing Jiancheng, Nanjing, China), and Fe^{2+} was measured colorimetrically (Elabscience). Manufacturer protocols were rigorously observed.

Statistical analysis

Results are reported as mean ±SD from a minimum of three ßindependent replicates. GraphPad Prism (v10.1; La Jolla, CA, USA) was used for analyses. Normality checks preceded testing. Differences between two groups were evaluated *via* Student's *t*-test or Mann-Whitney U test. For multiple groups, one-way ANOVA with Tukey's *post-hoc* test was applied. Statistical significance was set at $p<0.05$ (*$p<0.05$, **$p<0.01$, ***$p<0.001$, ****$p<0.0001$).

Results

Colchicine ameliorates severe acute pancreatitis and associated acute lung injury in rats

To evaluate the prophylactic efficacy of COL, Sprague-Dawley rats were administered COL (0.5 mg/kg/d) *via* intragastric gavage for seven consecutive days. One h after the final dose, SAP was induced by retrograde injection of 5% STC into the biliopancreatic duct. Samples were collected 24 h post-induction. The Sham group underwent gavage with physiological saline and sham surgery (Figure 1A). The 2D chemical structure of COL is present-

ed in Figure 1B.

Relative to the Sham group, SAP rats displayed severe acinar edema, hemorrhage, and necrosis in both gross assessments and H&E staining. Notably, these pathological changes were significantly mitigated in the SAP+COL group, which exhibited preserved tissue architecture and lower histopathological scores (Figure 1 C,D). Given that acute lung injury (ALI) is a frequent and fatal complication of SAP, we further examined pulmonary pathology. The SAP group displayed evident alveolar epithelial exudation, septal thickening, and erythrocyte infiltration into the alveolar spaces. Notably,

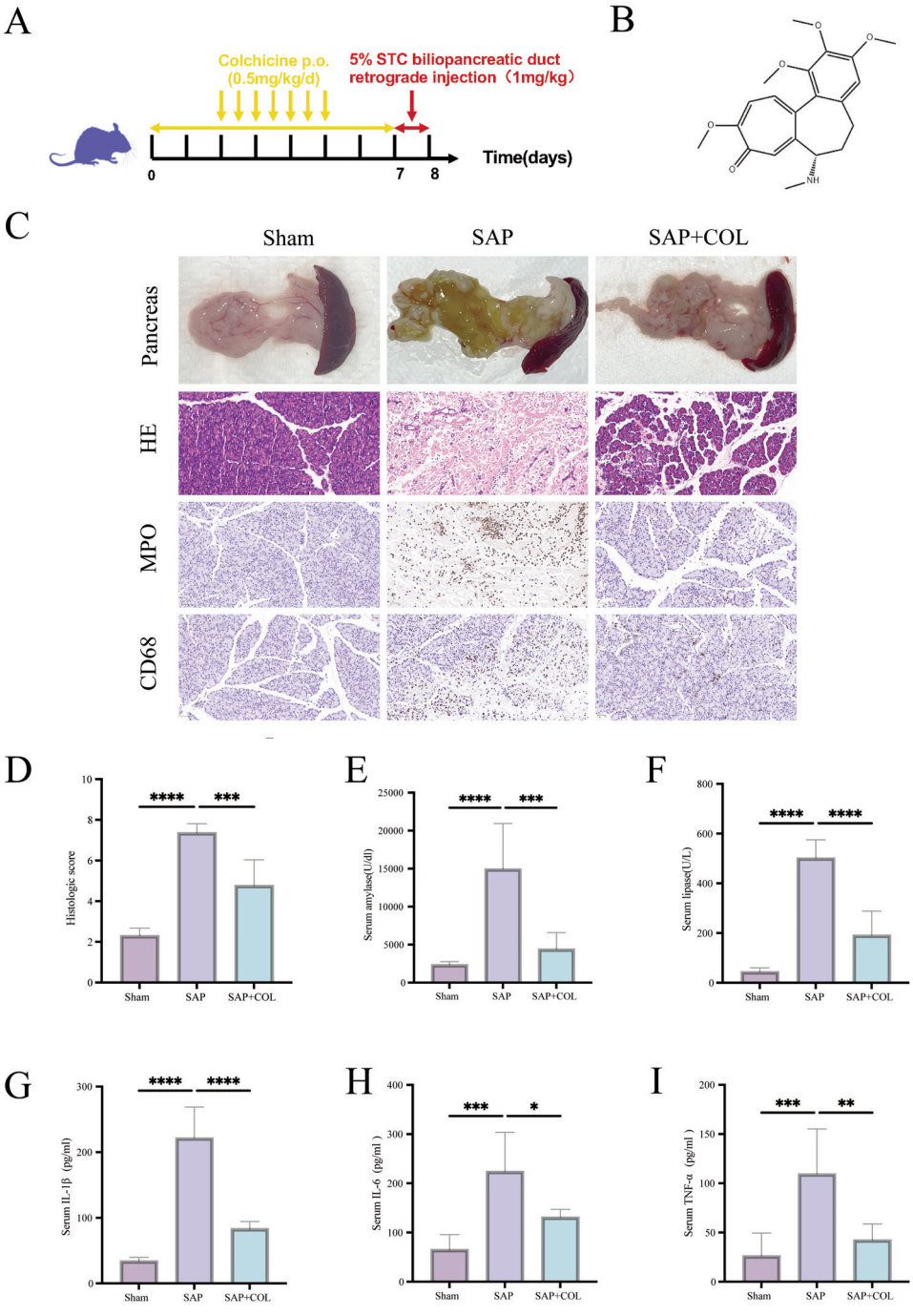

Figure 1. Colchicine ameliorates sodium taurocholate-induced severe acute pancreatitis (SAP) and associated pancreatic injury. **A**) Schematic diagram of the experimental design. **B**) 2D chemical structure of COL. **C**) Representative gross morphology of the pancreas (top), H&E staining (middle), and immunohistochemical (IHC) staining for the neutrophil marker MPO (brown) and macrophage marker CD68 (brown) (bottom) in the Sham, SAP, and SAP+COL groups; nuclei were counterstained with DAPI (blue). **D**) Histopathological scoring of pancreatic injury across groups. **E,F**) Serum amylase and lipase levels. **G-I**) Serum levels of pro-inflammatory cytokines IL-1β, IL-6, and TNF-α. Data are presented as mean ±SD (n=6). Magnification: 400×; scale bars: 50 μm.

COL pretreatment effectively mitigated these injuries (Figure S1A). IHC analysis further revealed a diffuse infiltration of neutrophils (MPO^+) and macrophages ($CD68^+$) in both the pancreas and lung of SAP rats. However, COL intervention significantly abrogated this inflammatory influx, as evidenced by the markedly reduced positivity rates for MPO^+ and $CD68^+$ (Figures 1C and S1B). Consistently, serum analysis demonstrated that COL treatment significantly attenuated the SAP-induced elevation of amylase and lipase, as well as pro-inflammatory cytokines interleukin 1β (IL-1β), interleukin 6 (IL-6), and tumor necrosis factor α (TNF-α), although levels

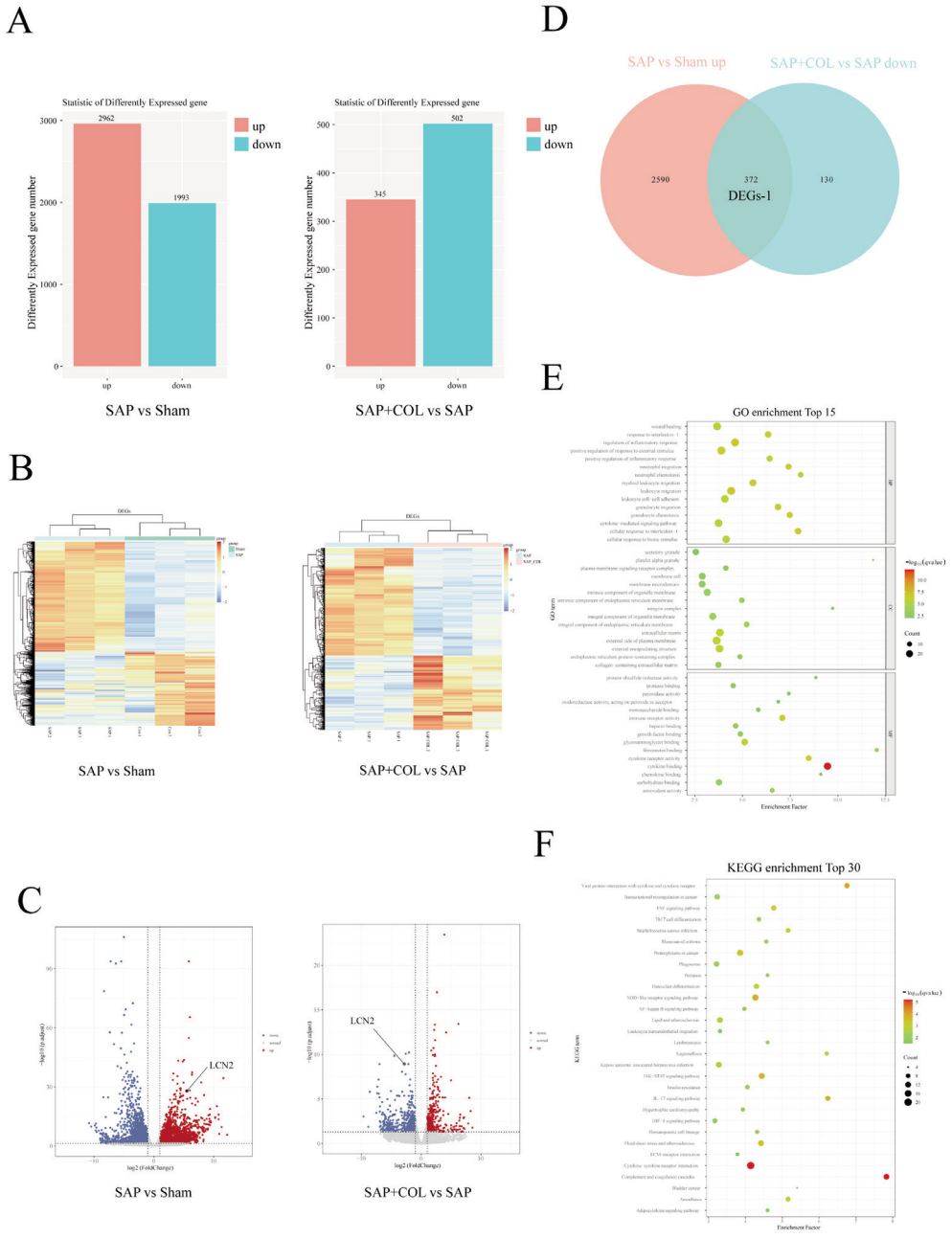

Figure 2. Transcriptomic profiling of the pancreas reveals colchicine-mediated gene expression alterations. **A**) Bar chart illustrating the number of differentially expressed genes (DEGs) in the SAP vs Sham (left) and SAP+COL vs SAP (right) comparisons; red bars indicate upregulation; blue bars indicate downregulation. **B**) Hierarchical clustering heatmap of DEGs across groups. Color gradient represents |log2 Fold Change|. **C**) Volcano plots displaying significant DEGs; red, upregulated; blue, downregulated; black, non-significant; thresholds: $p<0.05$ and |log2 Fold Change | >2. **D**) Venn diagram identifying the intersection of genes upregulated in SAP vs Sham and downregulated in SAP+COL vs SAP (designated as DEGs-1). **E**) Top 15 gene ontology (GO) enrichment terms for DEGs-1, categorized by biological process (BP), cellular component (CC), and molecular function (MF). **F**) Top 30 KEGG pathway enrichment analysis for DEGs-1.

remained higher than those in the Sham group (Figure 1 E-I). This anti-inflammatory efficacy was further confirmed by the reduced expression of IL-6 in the pancreas (Figure S1C). Collectively, these data confirm that prophylactic COL administration effectively attenuates STC-induced SAP and its associated complications, aligning with our previous observations.

Acquisition, processing of RNA-Seq data, and identification of DEGs

Building on the results, transcriptome sequencing was conducted on the pancreas (n=3) from the Sham, SAP, and SAP+COL groups by Oebiotech Co. After sequencing, the quality of the raw data was assessed, and unqualified reads were removed using Trimmomatic to enhance the accuracy of subsequent analyses. The R package limma (v 3.48.3) was then employed for differential expression analysis between the SAP and Sham, as well as between the SAP+COL and SAP, applying thresholds of $p<0.05$ and |log Fold Change| >2 to identify differentially expressed genes (DEGs). According to these criteria, a total of 2,962 genes were upregulated and 1,993 genes downregulated in SAP *vs* Sham. Following COL treatment, 345 genes were upregulated and 502 genes downregulated (Figure 2A), with results visually represented in heatmaps and volcano plots (Figure 2 B,C).

GO and KEGG pathway enrichment analyses of DEGs

To identify key genes associated with the therapeutic efficacy of COL, we performed an intersection analysis of the transcriptomic profiles. Specifically, genes upregulated in the SAP *vs* Sham comparison were intersected with those downregulated in the SAP+COL *vs* SAP comparison, yielding 372 overlapping DEGs (designated as DEGs-1). Conversely, genes downregulated in the SAP *vs* Sham comparison were intersected with those upregulated in the SAP+COL *vs* SAP comparison, resulting in 275 overlapping DEGs (designated as DEGs-2). These intersections are visualized *via* Venn diagrams (Figures 2D and S2A). Additionally, the top 10 most significantly dysregulated genes within DEGs-1 and DEGs-2 for both comparison groups are detailed in Tables S1 and S2.

To clarify the biological functions of these genes, gene ontology (GO) annotation and Kyoto Encyclopedia of Genes and Genomes (KEGG) pathway enrichment analyses were conducted on DEGs-1 and DEGs-2 using the R package (v3.19). For DEGs-1, GO analysis revealed a strong association with inflammatory processes. In the biological process (BP) category, terms were enriched in the *regulation of inflammatory response*, *leukocyte migration*, and *positive regulation of response to external stimulus*. The cellular component (CC) category highlighted enrichments in the *external side of plasma membrane*, *extracellular matrix*, and *external encapsulating structure*. Regarding molecular function (MF), the terms were primarily associated with *cytokine binding* (Figure 2E). Furthermore, KEGG pathway analysis demonstrated that DEGs-1 were robustly associated with critical inflammatory signaling cascades, including the *TNF signaling pathway*, *NOD-like receptor signaling pathway*, *NF-kappa B signaling pathway*, and *IL-17 signaling pathway* (Figure 2F). As DEGs-2 are not the main focus of this study, their GO annotation and KEGG pathway analysis results are provided in Figure S2 B,C.

Identification of LCN2 as a pivotal therapeutic target of colchicine in SAP

To elucidate the interactome of the DEGs-1 subset and identify potential hub genes, a protein-protein interaction (PPI) network was constructed using the STRING database. This analysis generated a complex network comprising 223 nodes and 1,131 edges (Figure 3A). Subsequently, we employed the CytoHubba plugin in Cytoscape to calculate topological features using five distinct algorithms: closeness, degree, EPC, MNC, and radiality. The top 20 ranked genes from each algorithm were identified for further scrutiny (Figure 3 B-F). Concurrently, modular analysis via the MCODE plugin revealed 30 significant functional clustering modules (Figure 3G). An intersection analysis of the top-ranked genes from the five algorithms and the MCODE modules yielded 17 core hub genes (Figure 3H, Table S3).

To bridge the gap between bioinformatics predictions and clinical applicability, we integrated network pharmacology to map the drug-disease interaction landscape. We identified 3,925 SAP-associated targets and 290 COL-associated targets. A Venn diagram intersection of the 17 hub genes with the overlapping drug-disease targets highlighted LCN2 and MMP9 as the two most promising candidates for COL-mediated intervention (Figure 3I).

To determine which of these two candidates served as the primary functional target of COL, we assessed the expression of LCN2 and MMP9 *in vivo* qRT-PCR and IHC. The results demonstrated that LCN2 expression was markedly upregulated in the SAP group and significantly suppressed by COL treatment at both the mRNA and protein levels. In contrast, while *MMP9* levels were elevated in the SAP group, COL treatment failed to significantly attenuate its expression (Figure 4 C-I and Figure S3 A,B). This discrepancy suggests that *MMP9* transcriptional activation during SAP may be governed by redundant or alternative signaling pathways not primarily modulated by COL. Based on this differential regulation, we therefore prioritized LCN2 over MMP9 as the critical molecular target through which COL ameliorates SAP.

Colchicine suppresses LCN2 expression and secretion in SAP

To validate the clinical relevance of LCN2 in pancreatitis, we first analyzed the GSE194331 dataset from the NCBI GEO database. The analysis revealed a significant upregulation of *LCN2* mRNA in the SAP group compared to the Control group (Figure 4A), a finding further visualized by volcano plot analysis (Figure 4B). Notably, this upregulation in human SAP samples was consistent with the elevated LCN2 mRNA levels observed in our rat model (Figure 4C), providing cross-species validation that strengthens the translational relevance of our findings. We subsequently assessed LCN2 protein dynamics *via* Western blot and IHC. Consistent with the transcriptional data, LCN2 protein levels were markedly elevated in the SAP group but were significantly suppressed following prophylactic COL administration (Figure 4 D,E,H). Given that LCN2 is a secretory lipocalin, we further quantified its levels in both pancreatic homogenates and serum using ELISA. A similar expression pattern was observed: systemic and local LCN2 levels surged in the SAP group and were attenuated by COL (Figure 4 F,G).

To precisely localize LCN2 expression within the pancreas, we performed double IF staining for LCN2 and Amylase (an acinar cell-specific marker). The results demonstrated distinct colocalization, identifying acinar cells as the primary source of LCN2 production. Following STC induction, acinar LCN2 fluorescence intensity increased sharply, whereas COL pretreatment significantly abrogated this upregulation (Figure 4I). Collectively, these data provide robust evidence that prophylactic COL administration significantly inhibits the expression and secretion of LCN2 in pancreatic acinar cells during SAP.

Pancreatic overexpression of LCN2 antagonizes the therapeutic efficacy of colchicine by promoting ferroptosis

To functionally validate the mechanistic role of LCN2 in COL-mediated protection, we employed an adeno-associated virus (AAV) vector with pancreatic tropism (AAV/PAN) to specifically overexpress LCN2 in the pancreas. A CMV promoter-driven green fluorescent protein (AAV/PAN-CMV-GFP) construct was utilized to assess transduction efficiency. *In vivo* imaging and fluorescence microscopy of frozen sections confirmed robust viral transduction and high GFP expression specifically within the pancreas (Figure S4 A,B).

Rats were randomly allocated into five cohorts (n=5): Sham, SAP, SAP+COL, SAP+COL+OE-CTR (empty vector), and SAP+COL+OE-LCN2. Rats in the overexpression groups received intraperitoneal injections of AAV/PAN constructs three weeks prior to modeling. Following a two-week incubation period to

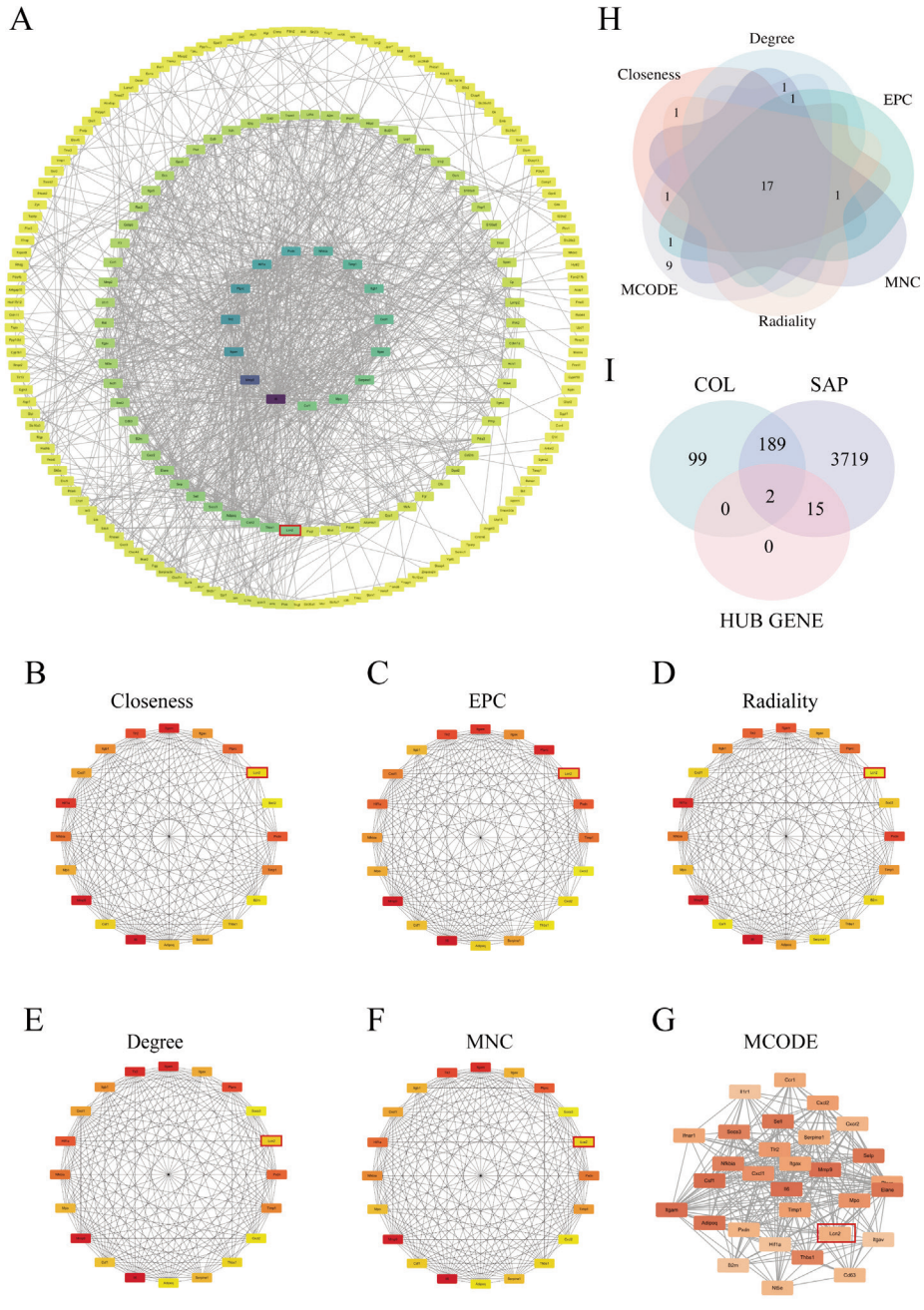

Figure 3. PPI analysis and Network pharmacology identify LCN2 as a pivotal therapeutic target. **A**) Protein-protein interaction (PPI) network of DEGs-1; node size and color intensity reflect connectivity. **B-F**) Top 20 hub genes identified by five topological algorithms: closeness, degree, EPC, MNC, and radiality. **G)** Thirty key clustering modules identified by MCODE analysis. **H**) Venn diagram showing the intersection of top-ranked genes from the five algorithms and MCODE modules. **I)** Venn diagram intersecting COL targets (blue), SAP disease targets (purple), and the identified Hub genes (pink) to pinpoint potential candidates.

allow for viral expression, rats underwent the standard COL pretreatment (1 week) followed by STC induction (24 h), as illustrated in the experimental timeline (Figure 5A). Western blot analysis confirmed the successful overexpression of LCN2 in the SAP+COL+OE-LCN2 group (Figure S4 C,D).

We observed that LCN2 overexpression significantly abrogated the therapeutic benefits of COL (Figure 5 B-H). Compared to the SAP+COL+OE-CTR group, the SAP+COL+OE-LCN2 group exhibited exacerbated pancreas pathology, characterized by diffuse acinar necrosis, vacuolization, hemorrhage, and elevated histopathological scores (Figure 5 B,C). This deterioration was accompanied by intensified infiltration of neutrophils and macrophages (Figure 5B) and a resurgence of serum amylase and lipase levels (Figure 5 D,E). Furthermore, the release of pro-inflammatory cytokines (IL-1β, IL-6, TNF-α), a hallmark of the transition from local inflammation to SIRS, was significantly re-elevated in the OE-LCN2 group (Figure 5 F-H). These data indicate that high levels of LCN2 are sufficient to reverse the anti-inflammatory protection conferred by COL.

Given the established link between LCN2 and ferroptosis - where trypsin activation exacerbates acinar cell ferroptosis- we hypothesized that COL functions by suppressing LCN2-dependent ferroptosis. To test this, we analyzed ferroptosis markers across the five groups. COL treatment effectively restored the GSH/ GSSG (oxidized glutathione) ratio and reduced levels of MDA and ferrous iron (Fe^{2+}). However, LCN2 overexpression nullified these protective effects, driving a significant reduction in GSH/GSSG and re-accumulation of MDA and Fe^{2+} (Figure 6 A-C). Consistent with this, immunofluorescence staining for ROS revealed that while COL suppressed the oxidative stress induced by SAP, LCN2 overexpression provoked a massive re-accumulation of ROS (Figure 6D). Molecularly, COL normally upregulates the anti-ferroptotic proteins ferritin heavy chain (FTH) and GPX4 while downregulating the pro-ferroptotic marker cyclooxygenase 2(COX2). Strikingly, LCN2 overexpression reversed this phenotype, leading to increased COX2 and diminished FTH and GPX4 expression (Figure 6 E-I).

To definitively establish that the LCN2-induced exacerbation relies on the ferroptosis pathway, we introduced a rescue group: SAP+COL+OE-LCN2+Fer-1, treating rats with the specific ferroptosis inhibitor Fer-1 (Figure 5A). Consistent with our hypothesis, Fer-1 treatment effectively rescued the deleterious phenotype caused by LCN2 overexpression. In this group, acinar necrosis and inflammatory infiltration were attenuated, and serum markers of injury and inflammation were significantly reduced compared to the SAP+COL+OE-LCN2 group (Figure 5 B-H). Mechanistically, Fer-1 restored the antioxidant defenses (GSH/GSSG, GPX4, FTH) and suppressed lipid peroxidation signals (MDA, Fe^{2+}, ROS, COX2) (Figure 6 A-I). Notably, Fer-1 administration did not alter LCN2 protein levels (Figure 6 E,F), indicating that LCN2 functions as an upstream regulator of the ferroptotic cascade. Collectively, these findings demonstrate that COL mitigates SAP by downregulating LCN2, which in turn prevents ferroptosis-driven acinar cell death.

Colchicine inhibits ferroptosis in SAP *via* the LCN2/MAPK/ERK signaling axis

Accumulating evidence implicates the mitogen-activated protein kinase (MAPK)/extracellular regulated kinase (ERK) signaling pathway as a critical driver in the pathogenesis of acute pancreatitis.[17,18] Notably, Wang *et al*. demonstrated that silencing LCN2 disrupts ferroptosis-mediated inflammation and oxidative stress by suppressing MAPK/ERK transduction.[19] Based on these precedents, we hypothesized that the mechanism by which LCN2 mediates COL in alleviating SAP is through the regulation of ferroptosis by LCN2 *via* the MAPK/ERK axis.

Western blot analysis revealed that SAP induction significantly triggered ERK1/2 phosphorylation (p-ERK1/2) compared to the Sham group. COL treatment effectively suppressed this activation, whereas LCN2 overexpression significantly reactivated ERK1/2 phosphorylation, overriding the suppressive effect of COL. To definitively delineate the signaling hierarchy, we employed PD98059, a highly specific ERK1/2 inhibitor, in the context of LCN2 overexpression (Figure 7A). We found that pharmacological inhibition of ERK1/2 mirrored the protective effects of the ferroptosis inhibitor Fer-1, effectively counteracting the pathological exacerbation caused by LCN2 overexpression. Compared to the SAP+COL+OE-LCN2 group, co-treatment with PD98059 significantly alleviated pancreas histopathological injury, reducing edema, hemorrhage, necrosis, and inflammatory scores (Figure 7 B,C). This was accompanied by a marked reduction in immune cell infiltration (decreased MPO and CD68 positivity) and a decline in serum amylase, lipase, and pro-inflammatory cytokines (IL-1β, IL-6, TNF-α) (Figure 7 D-H). Furthermore, PD98059 treatment successfully rescued the ferroptotic phenotype induced by LCN2. It restored the GSH/GSSG balance and reduced intracellular accumulation of MDA and Fe^{2+} (Figure 8 A-C). Fluorescence imaging confirmed that PD98059 significantly suppressed ROS generation (Figure 8D). At the protein level, PD98059 reversed the LCN2-induced upregulation of COX2 and the downregulation of FTH and GPX4 (Figure 8 E-J). Crucially, PD98059 administration did not alter the protein expression levels of LCN2 itself (Figure 8 E,F), confirming that MAPK/ERK signaling functions downstream of LCN2 in this pathological cascade. In summary, these findings substantiate a defined molecular mechanism: COL ameliorates SAP by downregulating LCN2, which subsequently inactivates the MAPK/ERK pathway to block acinar cell ferroptosis. The proposed mechanism is schematically illustrated in Figure 9.

Discussion

Based on our previous findings that COL ameliorates SAP and associated acute lung injury by suppressing inflammation, apoptosis, and oxidative stress, this study employed an integrative approach combining bioinformatics and network pharmacology to further dissect the molecular mechanisms within the primary pancreas lesion. We demonstrate, for the first time, that COL effectively mitigates SAP by significantly downregulating Lipocalin-2 (LCN2), which subsequently inhibits the activation of the downstream MAPK/ERK signaling pathway, ultimately blocking the ferroptotic cascade in pancreatic acinar cells.

SAP is a rapid-onset, high-mortality clinical emergency characterized by initial acinar cell injury and the massive release of damage-associated molecular patterns (DAMPs).[20] This triggers the robust recruitment of neutrophils to the pancreas, precipitating a systemic inflammatory cascade. As a classical anti-gout agent, COL possesses well-established anti-inflammatory properties.[21] Tercan *et al*. reported that long-term COL treatment reduces CD62L expression on neutrophils, thereby impairing their migration and adhesion capabilities.[22] Furthermore, COL has been shown to modulate cytoskeletal rearrangement by downregulating *CDC42EP3*, further disrupting neutrophil function.[23] Consistent with these mechanisms, our results confirm that COL pretreatment significantly ameliorates pancreatic edema, hemorrhage, and necrosis while suppressing the infiltration of MPO^+ neutrophils and $CD68^+$ macrophages. These findings align with the drug's

canonical mechanism of inhibiting microtubule polymerization and blocking NLRP3 inflammasome activation.

To deeply elucidate its mechanism, we screened 17 hub genes *via* whole-transcriptome sequencing combined with five topological algorithms and the MCODE plugin. By intersecting these with COL-SAP targets obtained from network pharmacology, we ultimately identified LCN2 as the pivotal target for COL in the treatment of SAP. LCN2, also known as neutrophil gelatinase-associated lipocalin (NGAL), is a secretory protein originally isolated from the gelatinase subcellular compartments of human neutrophils.[24] Its upregulation is closely related to immune cell migration, localization, infiltration, and adhesion.[25] Schroll *et al*. showed that

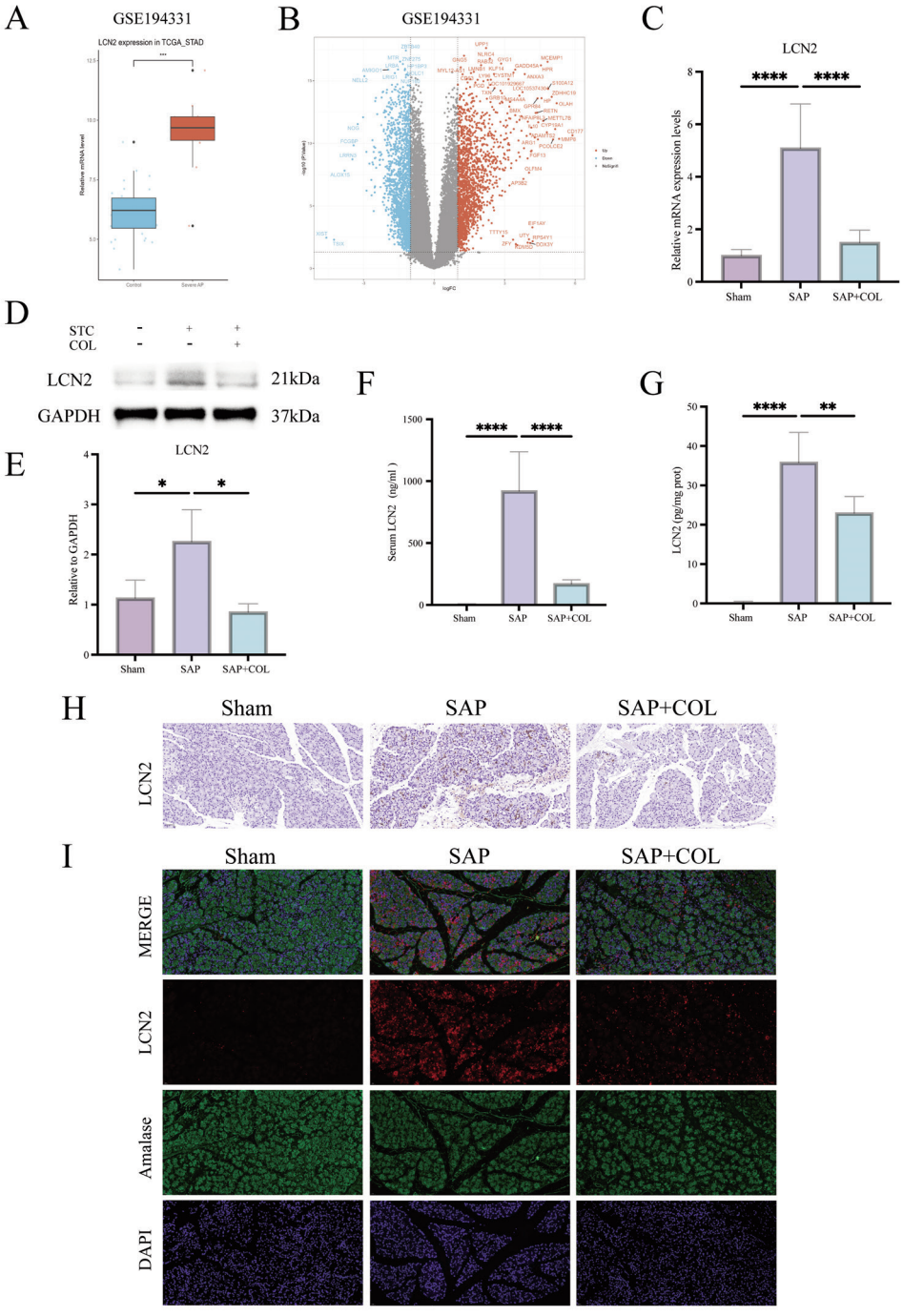

Figure 4. Multi-dimensional validation of LCN2 expression and localization. **A,B**) *LCN2* mRNA expression (FPKM) and volcano plot analysis from the GSE194331 dataset (control *vs* SAP). **C**) *LCN2* mRNA levels in rat pancreas measured by qRT-PCR. **D,E)** Representative Western blots and quantification of LCN2 protein levels in the pancreas. **F,G**) LCN2 protein levels in pancreas homogenates and serum measured by ELISA. **H**) Representative IHC staining for LCN2 (brown) in the pancreas. **I**) Representative double immunofluorescence staining for LCN2 (red) and the acinar cell marker alpha-amylase (green); nuclei were counterstained with DAPI (blue). Data are presented as mean ±SD (n=6). Magnification: 400×, scale bars: 50 μm.

LCN2 administration, whether intraperitoneal, intravenous, or intradermal, enhances leukocyte migration and infiltration.[26] Conversely, following inflammatory stimulation, *Lcn2* -/- mice exhibited significantly reduced neutrophil adhesion capacity and decreased expression of surface adhesion proteins and the chemokine receptor CXCR2.[26] Clinical studies suggest that LCN2 is correlated with the severity of acute pancreatitis (AP): urinary LCN2 levels are significantly elevated in the early stages of AP patients and are positively correlated with the severity of bilirubin and proteinuria.[27,28] Serum LCN2 concentration holds significant diagnostic value for the severity of early AP; its magnitude of elevation is substantially higher in SAP patients than in mild AP (MAP) cases, and it outperforms traditional scoring systems (such as APACHE II and Ranson scores) and biomarkers (such as C-

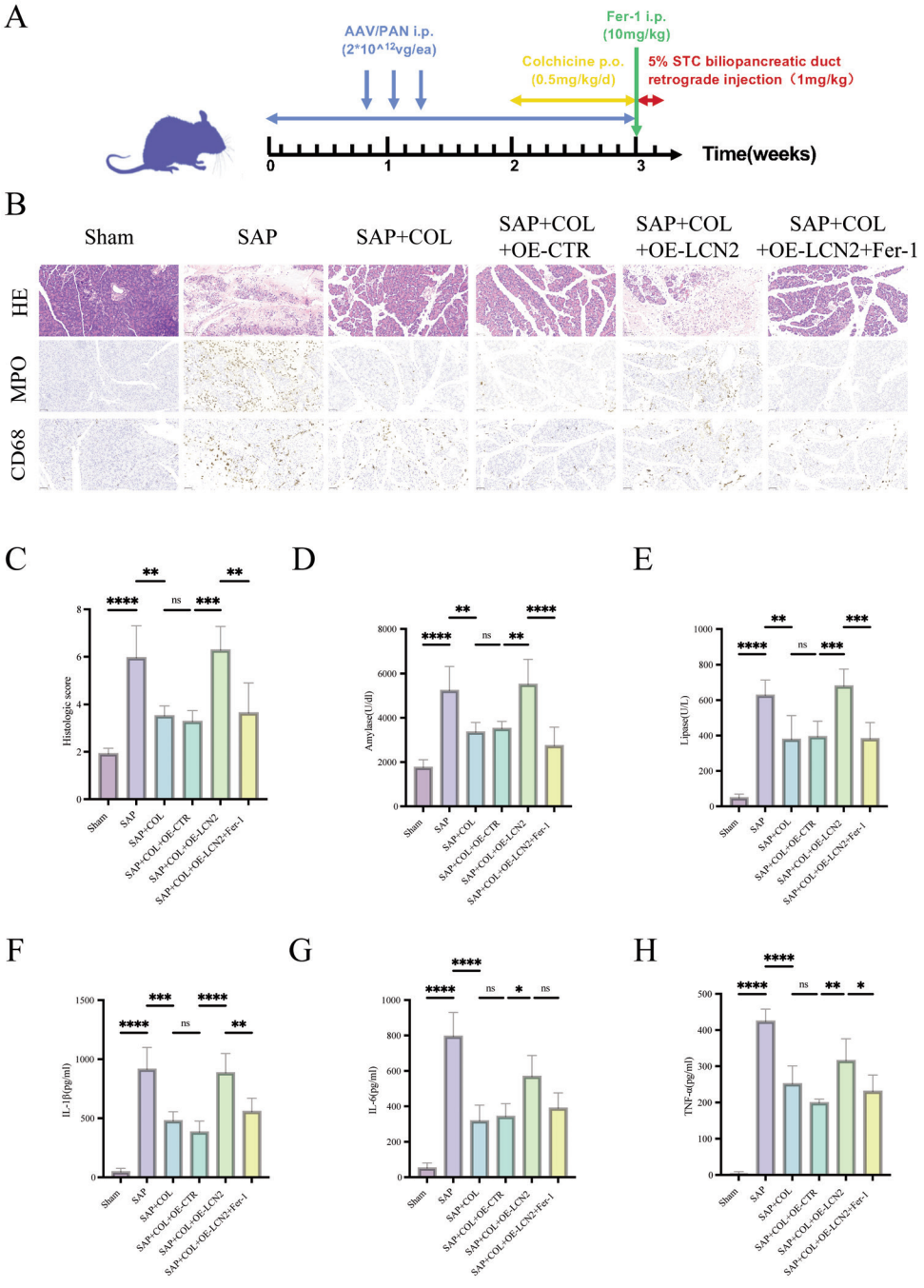

Figure 5. Pancreatic overexpression of LCN2 antagonizes the therapeutic efficacy of colchicine, which is rescued by ferrostatin-1. **A**) Schematic diagram of the rescue experiment design. **B**) Representative H&E staining and IHC staining for MPO (brown) and CD68 (brown) in the pancreas across six groups; nuclei were counterstained with DAPI (blue). **C**) Histopathological scoring of pancreatic injury. **D-H**) Serum levels of amylase, lipase, and pro-inflammatory cytokines (IL-1β, IL-6, TNF-α). Data are presented as mean ±SD (n=5). Magnification: 400×, scale bars: 50 μm.

reactive protein).[29-31] The severity of AP is not limited to the pancreas itself but lies in the distant organ damage it triggers.[32] Furthermore, LCN2 is an early, sensitive, and specific biomarker for acute kidney injury, and its sharp elevation may predict an increased risk of AP-associated renal injury.[33,34] Chakraborty *et al*. further indicated that high levels of NGAL can predict multiple organ failure (MOF) and poor prognosis in SAP patients.[31] Therefore, LCN2 may possess potential value in assessing the acute progression and long-term outcomes of AP.

However, the biological role of LCN2 is complex. On one hand, it acts as a pro-inflammatory amplifier; on the other hand, as an acute-phase protein, it functions in antimicrobial defense and iron homeostasis by sequestering bacterial siderophores.[35,36] Our core finding is that COL significantly suppresses the pathological

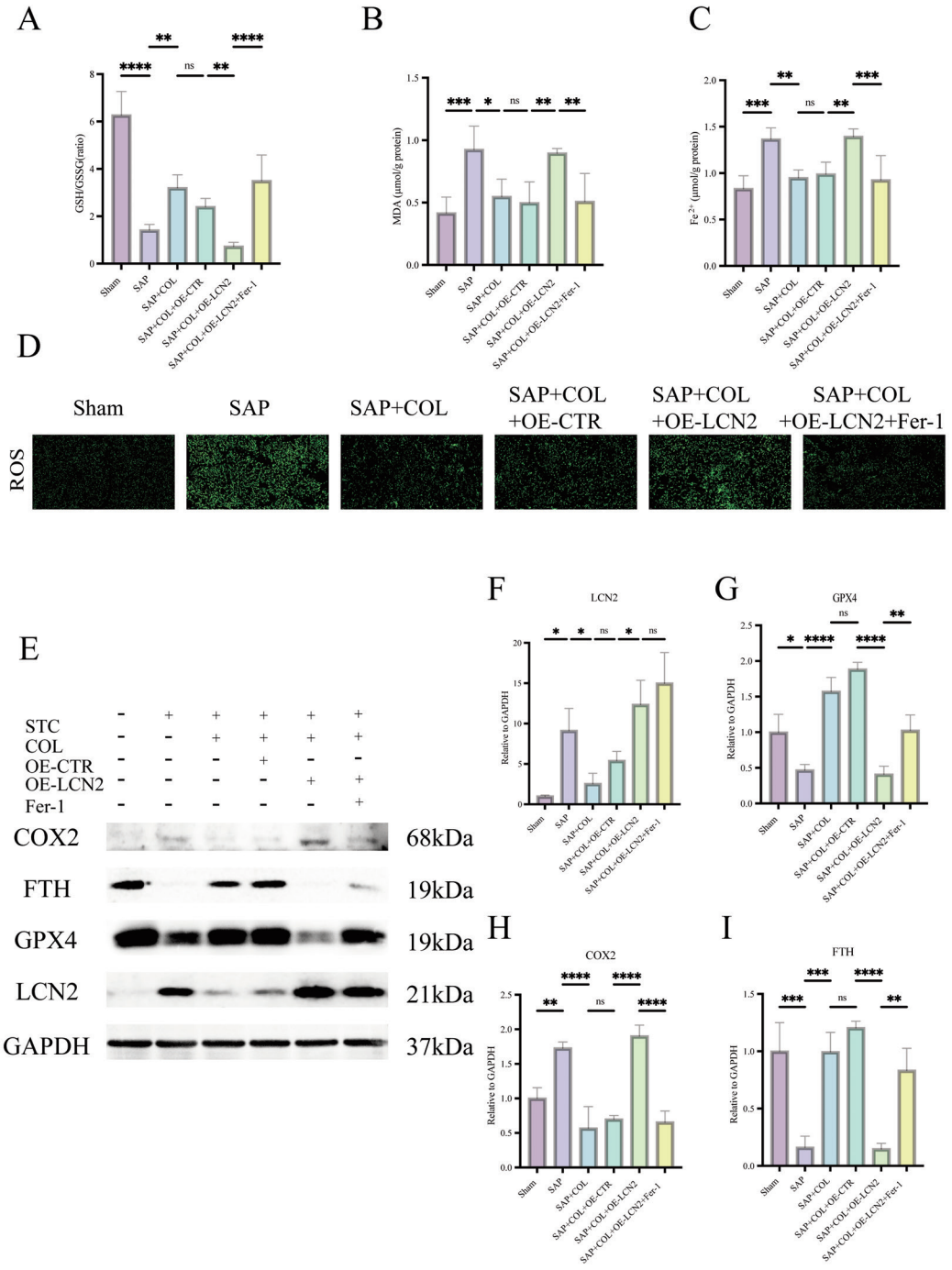

Figure 6. PLCN2 overexpression promotes pancreatic ferroptosis, an effect reversed by ferrostatin-1. **A-C**) Quantification of pancreatic GSH/GSSG ratio, MDA content, and Fe^{2+} levels. **D**) Representative fluorescence images of pancreatic ROS (green). **E-I**) Representative Western blots and quantification of LCN2, GPX4, COX2, and FTH protein levels. Data are presented as mean ±SD (n=5). Magnification: 400×, scale bars: 50 μm.

upregulation of LCN2 in SAP rats. This is corroborated by clinical data from the GSE194331 dataset, which shows elevated *LCN2* mRNA in SAP patients. Unlike the traditional view limiting colchicine's action to microtubule disruption and subsequent inhibition of neutrophil chemotaxis, our study establishes a novel direct link between COL and the transcriptional regulation of LCN2. Interestingly, although bioinformatics predicted both LCN2 and MMP9 as key targets, our *in vivo* data showed that COL failed to significantly suppress MMP9. While LCN2 is known to bind with MMP9 and enhance its stability and activity,[37,38] their regulation can be independent.[39] We postulate that in the intense inflammatory milieu of SAP, MMP9 expression is driven by redundant

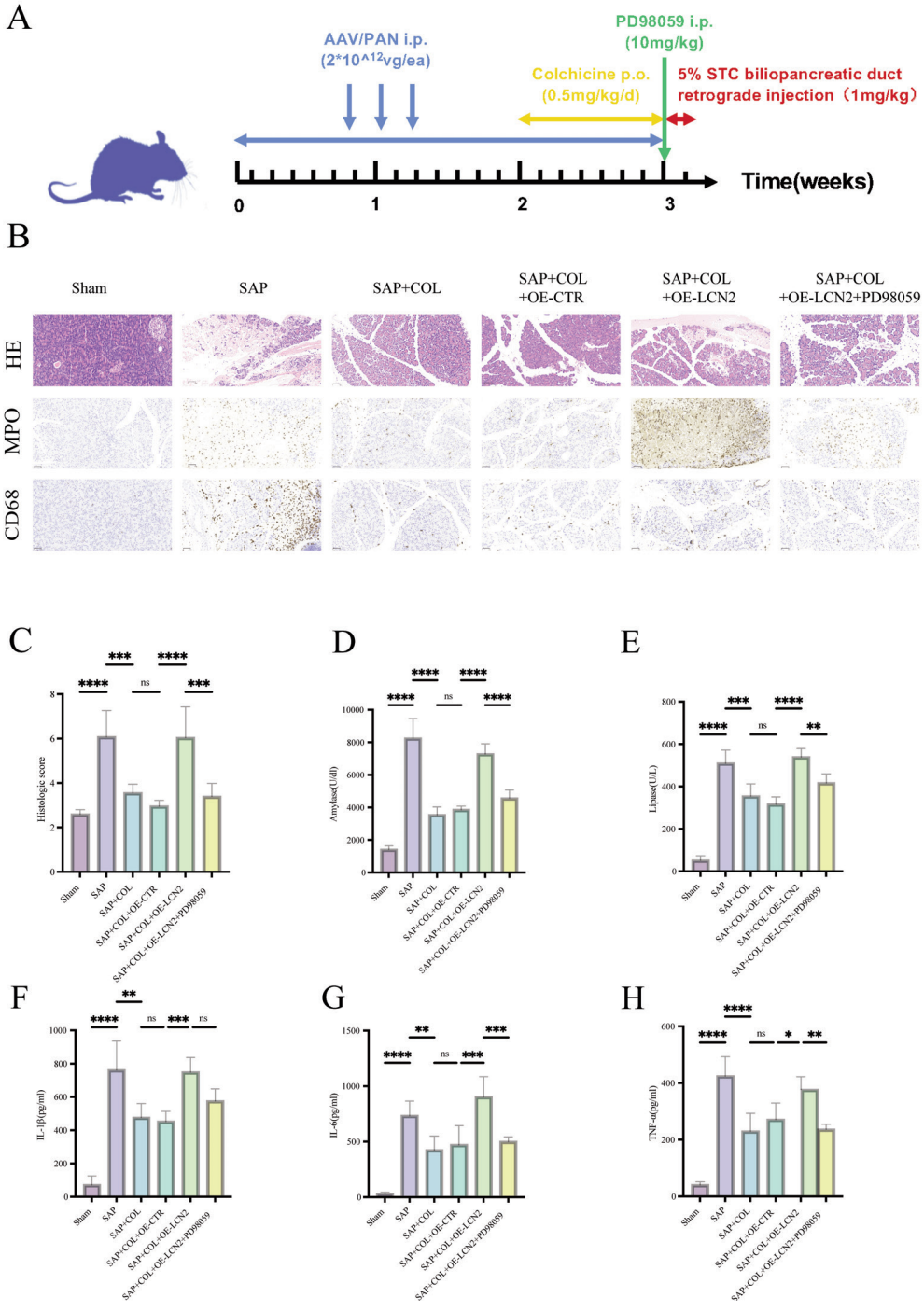

Figure 7. ERK1/2 inhibition (PD98059) rescues the LCN2-induced exacerbation of SAP. **A**) Schematic diagram of the experimental design involving PD98059. **B**) Representative H&E staining and IHC staining for MPO (brown) and CD68 (brown) across groups; nuclei were counterstained with DAPI (blue). **C**) Histopathological scoring of pancreatic injury across groups. **D-H**) Serum levels of amylase, lipase, and pro-inflammatory cytokines (IL-1β, IL-6, TNF-α). Data are presented as mean ±SD (n=5). Magnification: 400×, scale bars: 50 μm.

pathways (e.g., NF-κB), making it resistant to COL monotherapy. In contrast, LCN2 emerges as a more specific and sensitive target for COL.

Beyond its role in inflammation, emerging evidence implicates LCN2 in ferroptosis.[40] Ferroptosis is an iron-dependent form of regulated cell death characterized by the accumulation of lipid peroxides;[41] its occurrence is related to ROS accumulation caused by the failure of antioxidant systems (such as the GPX4 pathway), ultimately leading to cell membrane disintegration.[42] In the AP environment, pancreatic acinar cells are metabolically active and rich in polyunsaturated fatty acids, making them sensitive to oxidative stress and prone to ferroptosis.[43] The role of LCN2 in ferroptosis remains controversial: multiple studies explicitly state that LCN2 promotes ferroptosis by chelating siderophores and disrupting intracellular iron homeostasis. For instance, in an MPTP-induced Parkinson's disease mouse model, LCN2 within astrocytes facilitates iron endocytosis via its receptor 24p3R, thereby competitively inhibiting the binding of 24p3R to α-Syn, reducing the uptake and clearance of α-Syn by astrocytes.[44,45] Similarly, in an age-related heart failure model, butyrate reduces iron accumulation and inhibits ferroptosis by downregulating LCN2 expression in senescent cardiomyocytes.[46] However, some studies present the

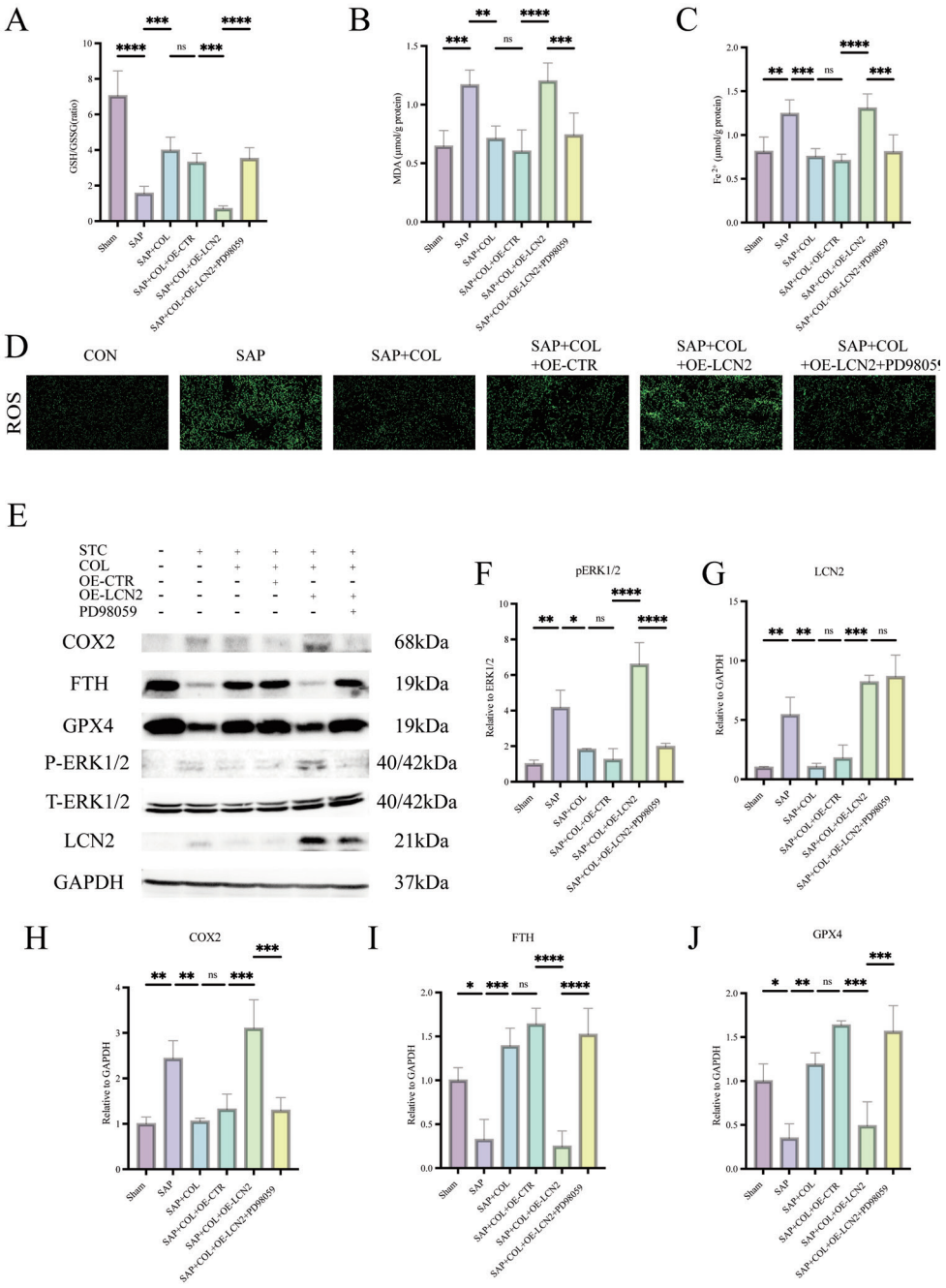

Figure 8. PD98059 suppresses LCN2 - driven ferroptosis in SAP. **A-C**) Quantification of pancreatic GSH/GSSG ratio, MDA content, and Fe^{2+} levels. **D**) Representative fluorescence images of pancreatic ROS (green). **E-J**) Representative Western blots and quantification of p-ERK1/2, LCN2, GPX4, COX2, and FTH protein levels. Data are presented as mean ±SD (n=5). Magnification: 400×, scale bars: 50 μm.

opposite view; Deng *et al*. reported that the transcription factor MafG interacts with MYH9 to upregulate LCN2 expression, which conversely inhibits ferroptosis in hepatic stellate cells to promote liver fibrosis.[47] Protein disulfide-isomerase A3 (PDIA3) is a key factor mediating ferroptosis susceptibility in glioblastoma cells. As an E3 ubiquitin ligase, NEDD4L mediates the ubiquitination of PDIA3 and enhances ferroptosis by downregulating the expression of LCN2. Consistently, Wang *et al.* reported that LCN2 inhibits ferroptosis in glioblastoma (GBM) cells *via* the receptor tyrosine kinase AXL.[48,49] These results suggest that the regulatory effect of LCN2 on ferroptosis is complex.

It is noteworthy that ferroptosis has been confirmed as one of the key mechanisms of pancreatic injury in SAP. The SAP period is usually accompanied by typical ferroptotic features within the pancreas, including the downregulation of GPX4 expression, elevation of the lipid peroxidation product MDA, and iron deposition.[50-52] In this study, LCN2 expression was upregulated in the pancreas of SAP rats, accompanied by alterations in ferroptosis-related indicators such as COX2, FTH, GPX4, as well as Fe^{2+}, MDA, GSH/GSSG, and ROS, which is consistent with the report by Zeng *et al*.[53] Crucially, AAV-mediated overexpression of LCN2antagonized the therapeutic effects of COL and reinstated ferroptosis, a phenotype that was rescuable by the ferroptosis inhibitor Fer-1. These data provide compelling evidence that COL alleviates SAP by suppressing LCN2-driven ferroptosis. Wang *et al.* proposed that LCN2 knockdown attenuates ferroptosis-related inflammation and oxidative stress by inhibiting the MAPK/ERK pathway,[18] and in an epilepsy model, sustained activation of MAPK/ERK signaling negatively regulates GPX4 and induces ferroptosis.[54] Our findings confirm this axis in pancreatic acinar cells: LCN2 overexpression reactivated MAPK/ERK signaling, promoting ferroptosis, whereas the ERK inhibitor PD98059 reversed these effects. Therefore, we can determine that in SAP, upregulated LCN2 activates the MAPK/ERK pathway, which downregulates GPX4 and triggers acinar cell ferroptosis; COL exerts its protective effect by blocking this specific signaling cascade.

The sample size for transcriptomic sequencing was relatively small, which may affect the generalizability and statistical power. Future studies with larger cohorts are warranted to validate the universality of these findings. Additionally, the clinical efficacy of COL in targeting LCN2 requires verification in large-scale clinical trials.

In summary, this study reaffirms the anti-inflammatory efficacy of COL in SAP and provides novel mechanistic insights. We identify the LCN2/MAPK/ERK/Ferroptosis axis as a critical therapeutic target of COL. Specifically, COL downregulates LCN2, thereby inhibiting MAPK/ERK activation and preventing acinar cell ferroptosis.

Acknowledgments

The authors thank Dr. Taojie Zhou (Shanghai Jiao Tong University) for his guidance and help in bioinformatics.

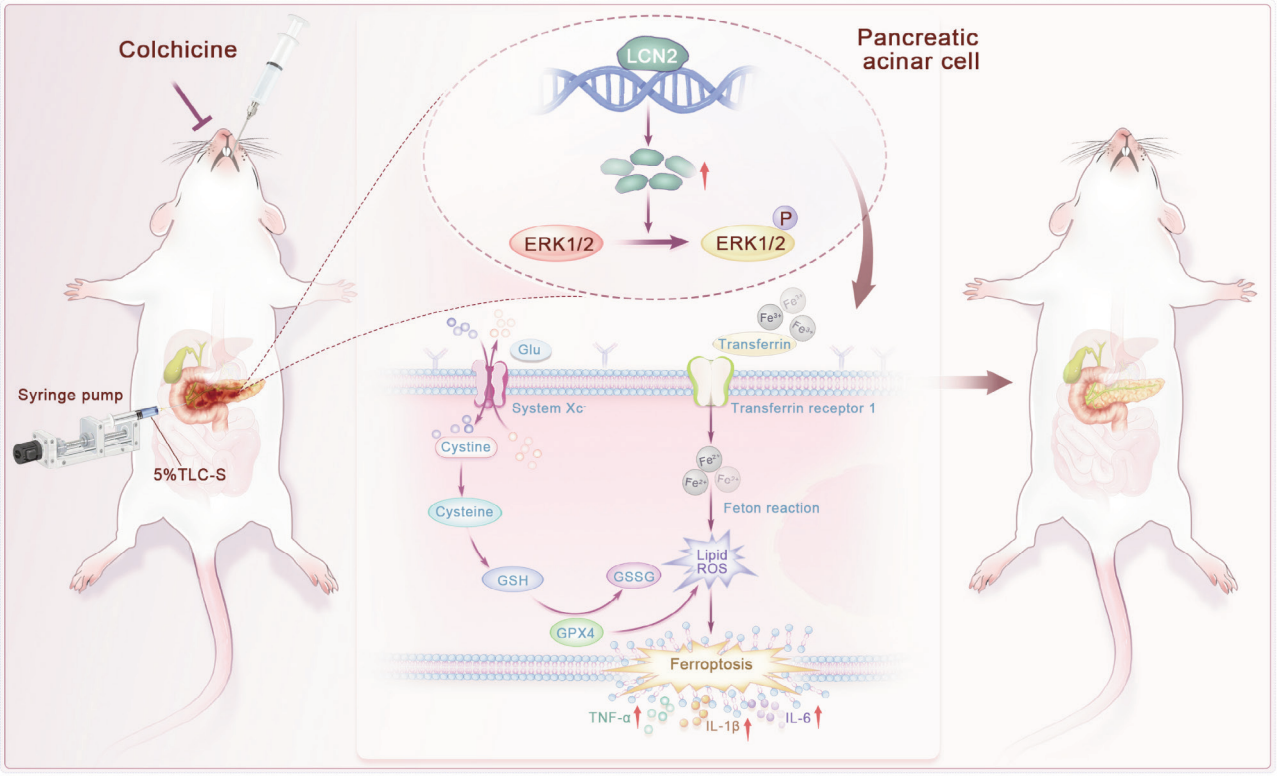

Figure 9. Schematic illustration of the mechanism. Upon SAP induction, upregulated LCN2 secretion activates the MAPK/ERK pathway (increased p-ERK1/2) in pancreatic acinar cells. This cascade disrupts System X_c^- function and Glutathione synthesis, impairing GPX4 activity and leading to lipid ROS accumulation. Concurrently, transferrin-mediated iron uptake promotes intracellular Fe^{2+} overload, fueling the Fenton reaction and lipid peroxidation, ultimately executing ferroptosis and releasing inflammatory cytokines (IL-1β, IL-6, TNF-α). COL exerts its therapeutic effect by downregulating LCN2 expression, thereby blocking this signaling axis and inhibiting ferroptosis.

References

1. Banks PA, Bollen TL, Dervenis C, Gooszen HG, Johnson CD, Sarr MG, et al. Classification of acute pancreatitis--2012: revision of the Atlanta classification and definitions by international consensus. Gut 2013;62:102-11.
2. Mederos MA, Reber HA, Girgis MD. Acute pancreatitis: a review. JAMA 2021;325:382-90.
3. Beger HG, Isenmann R. Diagnosis, objective assessment of severity, and management of acute pancreatitis. Santorini consensus conference. Int J Pancreatol 1999;25:195-210.
4. Huber SM, Navarini A, Brandt O, Müller S. Colchicine - Renaissance of an "ancient" drug. J Dtsch Dermatol Ges 2023;21:239-43.
5. Ellington E, Bastida J, Viladomat F, Codina C. Supercritical carbon dioxide extraction of colchicine and related alkaloids from seeds of Colchicum autumnale L. Phytochem Anal 2003;14:164-9.
6. Paschke S, Weidner AF, Paust T, Marti O, Beil M, Ben-Chetrit E. Technical advance: Inhibition of neutrophil chemotaxis by colchicine is modulated through viscoelastic properties of subcellular compartments. J Leukoc Biol 2013;94:1091-6.
7. Song P, Mao W, Chen Y, Liu Z, Chen Y. High-dose vitamin D Supplementation attenuates NLRP3 inflammasome-mediated oxidative stress in a novel murine model of comorbid asthma and osteoporosis induced by vitamin D deficiency. Iran J Allergy Asthma Immunol 2025;24:551-62.
8. Martínez GJ, Celermajer DS, Patel S. The NLRP3 inflammasome and the emerging role of colchicine to inhibit atherosclerosis-associated inflammation. Atherosclerosis 2018;269:262-71.
9. Zhang N, Zhao L, Li J, Li H, Chen Y. Harnessing nanotechnology for gout therapy: colchicine-loaded nanoparticles regulate macrophage polarization and reduce inflammation. Biomater Res 2024;28:0089.
10. Fan X, Wei C, Han Y. ALKBH5 Modulates asthma progression by downregulating n6-methyladenosine methylation. Iran J Allergy Asthma Immunol 2024;23:211-9.
11. Gu X, Huang Z, Ying X, Liu X, Ruan K, Hua S, et al. Ferroptosis exacerbates hyperlipidemic acute pancreatitis by enhancing lipid peroxidation and modulating the immune microenvironment. Cell Death Discov 2024;10:242.
12. Liu Y, Cui H, Mei C, Cui M, He Q, Wang Q, et al. Sirtuin4 alleviates severe acute pancreatitis by regulating HIF-1α/HO-1 mediated ferroptosis. Cell Death Dis 2023;14:694.
13. Xiao X, Yeoh BS, Vijay-Kumar M. Lipocalin 2: an emerging player in iron homeostasis and inflammation. Annu Rev Nutr 2017;37:103-30.
14. Liu J, Pang SY, Zhou SY, He QY, Zhao RY, Qu Y, et al. Lipocalin-2 aggravates blood-brain barrier dysfunction after intravenous thrombolysis by promoting endothelial cell ferroptosis via regulating the HMGB1/Nrf2/HO-1 pathway. Redox Biol 2024;76:103342.
15. Gupta U, Ghosh S, Wallace CT, Shang P, Xin Y, Nair AP, et al. Increased LCN2 (lipocalin 2) in the RPE decreases autophagy and activates inflammasome-ferroptosis processes in a mouse model of dry AMD. Autophagy 2023;19:92-111.
16. Wen Y, Li Y, Liu T, Huang L, Yao L, Deng D, et al. Chaiqin chengqi decoction treatment mitigates hypertriglyceridemia-associated acute pancreatitis by modulating liver-mediated glycerophospholipid metabolism. Phytomedicine 2024;134:155968.
17. Zhang B, Li SL, Xie HL, Fan JW, Gu CW, Kang C, et al. Effects of silencing the DUSP1 gene using lentiviral vector-mediated siRNA on the release of proinflammatory cytokines through regulation of the MAPK signaling pathway in mice with acute pancreatitis. Int J Mol Med 2018;41:2213-24.
18. Zhang H, Li Y, Li L, Liu H, Hu L, Dai Y, et al. Propylene glycol alginate sodium sulfate alleviates cerulein-induced acute pancreatitis by modulating the MEK/ERK pathway in mice. Mar Drugs 2017;15:45.
19. Wang X, Zhang C, Zou N, Chen Q, Wang C, Zhou X, et al. Lipocalin-2 silencing suppresses inflammation and oxidative stress of acute respiratory distress syndrome by ferroptosis via inhibition of MAPK/ERK pathway in neonatal mice. Bioengineered 2022;13:508-20.
20. Kang R, Lotze MT, Zeh HJ, Billiar TR, Tang D. Cell death and DAMPs in acute pancreatitis. Mol Med 2014;20:466-77.
21. Leung YY, Yao Hui LL, Kraus VB. Colchicine--Update on mechanisms of action and therapeutic uses. Semin Arthritis Rheum 2015;45:341-50.
22. Tercan H, van Broekhoven A, Bahrar H, Opstal T, Cossins BC, Rother N, et al. The effect of low-dose colchicine on the phenotype and function of neutrophils and monocytes in patients with chronic coronary artery disease: a double-blind randomized placebo-controlled cross-over study. Clin Pharmacol Ther 2024;116:1325-33.
23. He Y, Li D, Cook SL, Yoon MS, Kapoor A, Rao CV, et al. Mammalian target of rapamycin and Rictor control neutrophil chemotaxis by regulating Rac/Cdc42 activity and the actin cytoskeleton. Mol Biol Cell 2013;24:3369-80.
24. Flower DR, North AC, Sansom CE. The lipocalin protein family: structural and sequence overview. Biochim Biophys Acta 2000;1482:9-24.
25. Liu Y, Lin W, Bai Z, Ge Y, Xiao Y, Zhu F, et al. Lcn2 from neutrophil extracellular traps induces astrogliosis and post-stroke emotional disorders. Neuron 2025;113:4199-216.e8.
26. Schroll A, Eller K, Feistritzer C, Nairz M, Sonnweber T, Moser PA, et al. Lipocalin-2 ameliorates granulocyte functionality. Eur J Immunol 2012;42:3346-57.
27. Rybak K, Sporek M, Gala-Błądzińska A, Mazur-Laskowska M, Dumnicka P, Walocha J, et al. [Urinalysis in patients at the early stage of acute pancreatitis].[Article in Polish] Przegl Lek 2016;73:88-92.
28. Lipinski M, Rydzewska-Rosolowska A, Rydzewski A, Rydzewska G. Urinary neutrophil gelatinase-associated lipocalin as an early predictor of disease severity and mortality in acute pancreatitis. Pancreas 2015;44:448-52.
29. Sporek M, Dumnicka P, Gala-Błądzińska A, Mazur-Laskowska M, Walocha J, Ceranowicz P, et al. Determination of serum neutrophil gelatinase-associated lipocalin at the early stage of acute pancreatitis. Folia Med Cracov 2016;56:5-16.
30. Wood NJ. Pancreas: NGAL is a potential early diagnostic and prognostic biomarker of severe acute pancreatitis. Nat Rev Gastroenterol Hepatol 2010;7:589.
31. Chakraborty S, Kaur S, Muddana V, Sharma N, Wittel UA, Papachristou GI, et al. Elevated serum neutrophil gelatinase-associated lipocalin is an early predictor of severity and outcome in acute pancreatitis. Am J Gastroenterol 2010;105:2050-9.
32. Nickel F, Anthony Wise P. Acute pancreatitis and multiple organ failure-Who beats the odds? United European Gastroenterol J 2021;9:137-8.
33. Sporek M, Dumnicka P, Gala-Bladzinska A, Ceranowicz P, Warzecha Z, Dembinski A, et al. Angiopoietin-2 is an early indicator of acute pancreatic-renal syndrome in patients with acute pancreatitis. Mediators Inflamm 2016;2016:5780903.

34. Nga HS, Medeiros P, Menezes P, Bridi R, Balbi A, Ponce D. Sepsis and AKI in clinical emergency room patients: the role of urinary NGAL. Biomed Res Int 2015;2015:413751.
35. Goetz DH, Holmes MA, Borregaard N, Bluhm ME, Raymond KN, Strong RK. The neutrophil lipocalin NGAL is a bacteriostatic agent that interferes with siderophore-mediated iron acquisition. Mol Cell 2002;10:1033-43.
36. Flo TH, Smith KD, Sato S, Rodriguez DJ, Holmes MA, Strong RK, et al. Lipocalin 2 mediates an innate immune response to bacterial infection by sequestrating iron. Nature 2004;432:917-21.
37. Jaberi SA, Cohen A, D'Souza C, Abdulrazzaq YM, Ojha S, Bastaki S, et al. Lipocalin-2: Structure, function, distribution and role in metabolic disorders. Biomed Pharmacother 2021;142:112002.
38. Xia Q, Du Z, Chen M, Zhou X, Bai W, Zheng X, et al. A protein complex of LCN2, LOXL2 and MMP9 facilitates tumour metastasis in oesophageal cancer. Mol Oncol 2023;17:2451-71.
39. Liu Y, Shao YH, Zhang JM, Wang Y, Zhou M, Li HQ, et al. Macrophage CARD9 mediates cardiac injury following myocardial infarction through regulation of lipocalin 2 expression. Signal Transduct Target Ther 2023;8:394.
40. Schröder SK, Gasterich N, Weiskirchen S, Weiskirchen R. Lipocalin 2 receptors: facts, fictions, and myths. Front Immunol 2023;14:1229885.
41. Stockwell BR, Friedmann Angeli JP, Bayir H, Bush AI, Conrad M, Dixon SJ, et al. Ferroptosis: a regulated cell death nexus linking metabolism, redox biology, and disease. Cell 2017;171:273-85.
42. Dixon SJ, Lemberg KM, Lamprecht MR, Skouta R, Zaitsev EM, Gleason CE, et al. Ferroptosis: an iron-dependent form of nonapoptotic cell death. Cell 2012;149:1060-72.
43. Li H, Lin Y, Zhang L, Zhao J, Li P. Ferroptosis and its emerging roles in acute pancreatitis. Chin Med J (Engl) 2022;135:2026-34.
44. Jiao YY, Tian T, Zhu Z, Cao L, Liu Y, Wang RA, et al. Extracellular LCN2 binding to 24p3R in astrocytes impedes α-synuclein endocytosis in Parkinson's disease. Adv Sci (Weinh) 2025;12:e01694.
45. Langelueddecke C, Roussa E, Fenton RA, Wolff NA, Lee WK, Thévenod F. Lipocalin-2 (24p3/neutrophil gelatinase-associated lipocalin (NGAL)) receptor is expressed in distal nephron and mediates protein endocytosis. J Biol Chem 2012;287:159-69.
46. Zhang Y, Wei Y, Han X, Shi L, Yu H, Ji X, et al. Faecalibacterium prausnitzii prevents age-related heart failure by suppressing ferroptosis in cardiomyocytes through butyrate-mediated LCN2 regulation. Gut Microbes 2025;17:2505119.
47. Deng Y, Lu L, Zhu D, Zhang H, Fu Y, Tan Y, et al. MafG/MYH9-LCN2 axis promotes liver fibrosis through inhibiting ferroptosis of hepatic stellate cells. Cell Death Differ 2024;31:1127-39.
48. Zhang J, Wang W, Liu X, Lu P, Liu X, Nie Q, et al. PDIA3 inhibition facilitates sensitivity of IKE-induced ferroptosis via STAT3/LCN2 Axis to improve glioblastoma therapy. Adv Sci (Weinh) 2026;13:e14191.
49. Wang SZ, Timken JP, Hong ES, Kaur S, Newby E, Kay KE, et al. Lipocalin 2 orchestrates resistance to ferroptosis via AXL. Cell Rep 2026;45:116965.
50. Zhang R, Ling X, Guo X, Ding Z. CD36 Induces inflammation by promoting ferroptosis in pancreas, epididymal adipose tissue, and adipose tissue macrophages in obesity-related severe acute pancreatitis. Int J Mol Sci 2025;26.
51. Fang Z, Li J, Cao F, Li F. Integration of scRNA-Seq and bulk RNA-Seq reveals molecular characterization of the immune microenvironment in acute pancreatitis. Biomolecules 2022;13:78.
52. Xiang X, Xu M, Liu L, Meng N, Lei Y, Feng Y, et al. Liproxstatin-1 attenuates acute hypertriglyceridemic pancreatitis through inhibiting ferroptosis in rats. Sci Rep 2024;14:9548.
53. Zeng X, Chen W, Dai Q, He Y, Fu X, Liu J, et al. Nuclear protein 1 defends against acute pancreatitis by mitigating pancreatic acinar cell ferroptosis through the maintenance of cellular iron homeostasis. Toxicol Appl Pharmacol 2026;508:117720.
54. Li X, Quan P, Si Y, Liu F, Fan Y, Ding F, et al. The microRNA-211-5p/P2RX7/ERK/GPX4 axis regulates epilepsy-associated neuronal ferroptosis and oxidative stress. J Neuroinflammation 2024;21:13.

Online Supplementary Material
Figure S1. Colchicine mitigates SAP-associated ALI and inflammatory infiltration.
Figure S2. Functional enrichment analysis of DEGs-2.
Figure S3. In vivo validation of MMP9 expression.
Figure S4. Validation of AAV-mediated pancreas-specific LCN2 overexpression.
Table S1. Top 10 upregulated DEGs-1 and downregulated DEGs-2 between SAP group and CON group.
Table S2. Top 10 upregulated DEGs-2 and downregulated DEGs-1 between SAP+COL group and SAP group.
Table S3. Hub genes identified by overlap of top 20 genes from five algorithms and top 30 MCODE modules.

Received: 9 March 2026. Accepted: 2 April 2026.

Licensee PAGEPress, Italy
European Journal of Histochemistry 2026; 70:4557
doi:10.4081/ejh.2026.4557